THE MOST OBSCURED AGN IN THE CHANDRA/SWIRE SURVEY IN THE LOCKMAN HOLE[1]

M. Polletta[1], B.J. Wilkes[2], B. Siana[3], C.J. Lonsdale[1,4], R. Kilgard[2], D.L. Shupe[3], J. Surace[3], H.E. Smith[1], and F. Owen[5]

[1]Center for Astrophysics & Space Sciences, University of California, San Diego, La Jolla, CA 92093–0424, USA
[2]Harvard/Smithsonian Center for Astrophysics, 60 Garden Street, Cambridge, MA 02138, USA
[3]*Spitzer* Science Center, California Institute of Technology, 100-22, Pasadena, CA 91125, USA
[4]Infrared Processing & Analyis Center, California Institute of Technology, 100-22, Pasadena, CA 91125, USA
[5]National Radio Astronomy Observatory, P.O. Box O, Socorro, NM 87801, USA

ABSTRACT

The high sensitivity and spatial resolution of the *Spitzer* Space Telescope and of the *Chandra* X-ray Observatory are combined in the wide area (0.6 square degrees) *Chandra*/SWIRE survey in the Lockman Hole (10h45m, +59d) to investigate the properties of Active Galactic Nuclei (AGN). The X-ray and infrared data are used independently to select two samples of heavily obscured (Compton-thick) AGN candidates. The two selected samples contain 1) 5 X-ray sources with hard X-ray spectra and column densities $\geq 10^{24}\,\mathrm{cm}^{-2}$, and 2) 100 infrared sources with red and AGN-dominated infrared spectral energy distributions (SEDs). We estimate a surface density of at least 25 Compton-thick AGN per deg^2 detected in the IR in the *Chandra*/SWIRE field of which $\sim$40% show distinct AGN signatures in their optical/near-infrared SEDs, the remaining sources being dominated by the host-galaxy emission. Only $\sim$33% of all Compton-thick AGN are detected in the X-rays at our depth (F(0.3-8 keV)$>10^{-15}\,\mathrm{ergs\,cm}^{-2}\,\mathrm{s}^{-1}$). We report the discovery of the most luminous Compton-thick AGN at high-z currently known, SWIRE_J104409.95+585224.8 (z=2.54, $L_{bol} \simeq 10^{14}\mathrm{L}_\odot$). The properties of this source are discussed in detail with an analysis of its spectrum, SED, luminosity and black-hole mass.

Key words: galaxies: active; quasars: individual (SWIRE_J104409.95+585224.8); infrared: galaxies; X-rays: galaxies.

1. INTRODUCTION

The ubiquity of super-massive black-holes (SMBH) in galaxies, the correlation between their masses and the galaxy stellar mass (Ferrarese & Merrit , 2000) and the similarity between their space density (La Franca et al., 2005; Wolf, 2005) and the star-formation history of galaxies (Hartwick , 2004) strongly suggest that galaxy and AGN evolution are connected. Several current models attribute the link between the two processes to a merger event of large galaxies (Silk & Rees , 1998; Granato et al., 2004; Springel et al., 2005; Hopkins et al., 2005; Di Matteo et al., 2005; Cattaneo et al., 2005). During the merger, the SMBH and the host galaxy spheroid grow throughout vigorous star-formation episodes (Fabian , 1999). The merging system contains large amounts of gas and dust and the nucleus appears as heavily obscured. Both AGN and host-galaxy will experience major changes during this obscured phase in stellar mass, star-formation rate, and AGN luminosity. Many physical processes of this scenario remain to be explained and many predictions lack observational testing, especially for AGN in obscured phases which are hard to detect and identify.

The existence of a large population of obscured AGN is not only a model prediction, but it is also suggested by indirect observations like the shape of the X-ray background which is still largely unresolved at energies above 8 keV (Worsley et al., 2005) or the high fraction of obscured versus unobscured AGN (4:1) at low-z (Risaliti et al., 1999; Maiolino & Rieke, 1995; Piconcelli et al., 2003). Although these observations strongly suggest that obscured AGN are numerous and might even outnumber unobscured AGN, large and complete samples of obscured AGN are still missing.

In this work, we present a selection of the most obscured AGN, the so-called Compton-thick ($N_\mathrm{H} \geq 10^{24}\,\mathrm{cm}^{-2}$) AGN and provide statistical constraints on their surface density. Our analysis is based on observations performed with the *Spitzer* Space Telescope as part

of the *Spitzer* Wide-Area Infrared Extragalactic Survey (SWIRE) (Lonsdale et al., 2003, 2004) and with the *Chandra* X-ray Observatory in a wide area (0.6 deg^2) in the Lockman Hole, the *Chandra*/SWIRE field.

2. OBSERVATIONS

The *Chandra*/SWIRE survey was performed in the northern part of the Lockman Hole which is the largest field (11 deg^2 centered at 10^h45^m, $+58°$) of the five observed by the SWIRE Project. The *Chandra*/SWIRE field (0.6 deg^2 centered at 10^h45^m, $+59°$) has been selected for deep multi-wavelength observations. The *Spitzer* data include images obtained with the Infrared Array Camera (IRAC) (Fazio et al., 2004) and the Multiband Imaging Photometer (MIPS) (Rieke et al., 2004). The 5σ limits of the *Spitzer* data are 5, 9, 43, 40 and 230 μJy at 3.6, 4.5, 5.8, 8.0 and 24μm, respectively (Surace et al., 2005). The infrared (IR) catalog contains 41,262 sources. Optical imaging in U, g', r', and i' was obtained with the Mosaic Camera at the Kitt Peak National Observatory (KPNO) Mayall 4-mt Telescope. The 5σ limiting Vega magnitudes are 24.8 (U), 25.9 (g'), 25.2 (r'), and 24.4 (i'). The optical catalog contains 77,355 sources and 31'106 sources are also detected in the IR. Thanks to the lack of nearby moderate brightness radio sources in the *Chandra*/SWIRE field, an extremely deep radio survey at 20 cm was also performed (Owen et al., in prep.). A 1.4 GHz radio map covering $40' \times 40'$ in the *Chandra*/SWIRE field, was obtained at the Very Large Array (VLA) with a root-mean-squared (rms) noise in the center of the radio image of 2.7 μJy. There are 2052 radio sources in the entire field and 2000 are also detected in the IR with IRAC. *Chandra* Advanced CCD Imaging Spectrometer (ACIS-I) (Weisskopf, O'dell, & van Speybroeck, 1996) observations were performed in a 3×3 raster for a total area of 0.6 deg^2 centered at $10^h 46^m$, $+59° 01'$. The exposure time for each pointing was $\sim$70 ksecs, reaching a broad-band (0.3–8 keV) flux limit of $\sim 10^{-15}$ ergs cm^{-2} s^{-1}. A total of 792 sources were detected. An IR counterpart is matched to 774 (98%) sources, 640 (81%) of which are also detected in the optical images. The fraction of X-ray sources that are radio detected is 50% within $10'$ from the center of the radio field and 27% in the whole field.

3. COMPTON-THICK AGN SELECTION

In the following sections, we present two methods for selecting AGN with extreme column densities ($N_H \geq 10^{24}$ cm^{-2}), the so called Compton-thick AGN, one is based on the X-ray properties and the other on the optical-IR properties. Since the methods require redshifts, and spectroscopic redshifts are available for only a small fraction of sources, we supplement the spectroscopic redshifts with photometric redshifts. Photometric redshifts were derived using the code HYPERZ (Bolzonella et al.,

2000). We use a library 24 galaxy templates which includes 9 normal galaxy, 3 starburst, and 12 AGN templates and cover the wavelength range from 1000Å to 500μm (Polletta et al., in preparation).

3.1. X-ray selected obscured AGN

Obscured AGN were selected among the X-ray sources based on the estimated column density. This selection is biased against Compton-thick AGN in which the primary radiation is completely obscured at the observed energies (<8 keV) and only the warm scattered component is observed. This bias is less important for high-z sources where the observed radiation is emitted at higher energies in the source rest-frame. In order to derive the
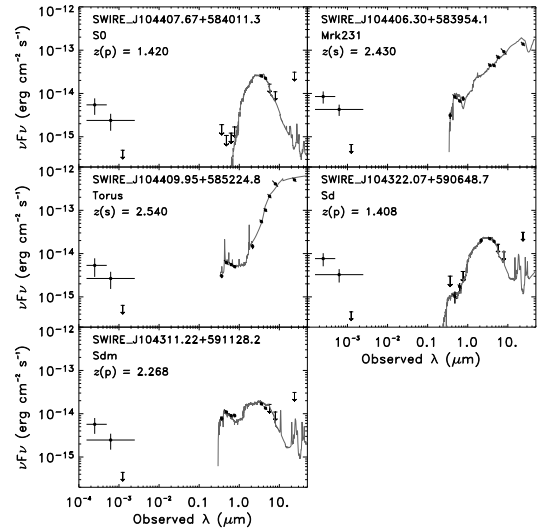

Figure 1. SED in $\nu F\nu$ of 5 X-ray selected Compton-thick AGN (full circles). The source names are reported on the upper-left corner of each panel. Downward arrows indicate upper limits at the completeness limit in the optical and at 5σ in the IR. The broad-, hard-, and soft-X-ray fluxes are shown as full circles. The X-ray fluxes are derived assuming an absorbed power-law model with photon index, Γ, equal to 1.7 and Galactic absorption, $N_H = 6 \times 10^{19}$ cm^{-2}. A downward arrow at 1σ limit is used in the X-rays when the counts are less than 1σ. The best-fit template for each object is shown as a grey curve and the template name is reported in each panel. The spectroscopic (z_s) or photometric (z_p) redshift of each object is also reported.

amount of absorption, spectral files were created, for each source, using Sherpa (Freeman et al., 2001) simulations. In the simulations, we assumed an absorbed power-law model with a fixed photon-index $\Gamma = 1.7$, corresponding to the observed mean for AGN (Nandra & Pounds, 1994), and a range of column densities from $N_H = 10^{19}$ cm^{-2} to $10^{24.5}$ cm^{-2}. Each spectrum and the estimated local background as derived applying the Bayesian method (van Dyk et al., 2004), were used as

Table 1. Properties of X-ray selected Compton-thick AGN.

Source Name	F(24μm) (mJy)	F$_{0.3-8keV}^{a}$	HR	z	N$_{H}^{obs,b}$	N$_{H}^{rest,c}$	Log(L)^{d}
SWIREJ104407.67+584011.3	<0.23	24±10	$1.00_{-0.13}^{+0.0}$	1.42	$20_{-11}^{+\infty}$	$200_{-109}^{+\infty}$	45.5
SWIREJ104406.30+583954.1	1.099	43±12	$0.61_{-0.23}^{+0.21}$	2.43^{e}	4_{-1}^{+3}	99_{-25}^{+74}	45.7
SWIREJ104409.95+585224.8	4.011	27±11	$0.85_{-0.39}^{+0.06}$	2.54^{e}	8_{-5}^{+2}	214_{-134}^{+54}	46.1
SWIREJ104322.07+590648.7	<0.23	33±11	$1.00_{-0.04}^{+0.0}$	1.41	$30_{-10}^{+\infty}$	$312_{-104}^{+\infty}$	45.6
SWIREJ104311.22+591128.2	<0.23	25±10	$1.00_{-0.15}^{+0.0}$	2.27	30_{-23}^{+40}	863_{-662}^{+1151}	45.9

^{a} X-ray flux in 10^{-16} ergs cm^{-2} s^{-1} derived assuming an absorbed power-law model with Γ=1.7 and Galactic absorption (N$_{H}$=6×10^{19} cm^{-2}). Uncertainties reflect only the statistical errors from the observed counts and do not include uncertainties in the spectral model. ^{b} N$_{H}$ in the observer rest-frame in 10^{22} cm^{-2}. ^{c} Effective N$_{H}$ in 10^{22} cm^{-2}. ^{d} Absorption-corrected rest-frame 0.3-8 keV luminosity in ergs s^{-1}. ^{e} Spectroscopic z.

input to MARX[1] to create a simulated data set. Hardness ratios (HR[2]) were calculated from the simulations of each source for all column densities. The column density, N$_{H}^{obs}$, of each source was determined by comparing the observed HR with the values derived from the simulation. The effective hydrogen column densities, N$_{H}^{rest}$, were then derived after correcting for the redshift of the sources as N$_{H}^{rest}$=N$_{H}^{obs}$ × $(1+z)^{2.6}$ (Longair, 1992). We found 5 X-ray sources with an intrinsic N$_{H}^{rest} \geq 10^{24}$ cm^{-2}. Source names, coordinates and X-ray properties (broad-band X-ray flux, HR, column density and absorption corrected broad band luminosity) are listed in Table 1, and their spectral energy distributions (SEDs) are shown in Fig. 1. Two sources show a distinct AGN signature in their optical/near-IR SED, while the other three sources are dominated by starlight in the optical and near-IR. The estimated column densities and absorption-corrected X-ray (0.3-8 keV) luminosities imply that these are all Compton-thick quasars.

3.2. IR-selected obscured AGN

In order to estimate the number of Compton-thick AGN detected in the IR, but missed in the X-rays at our limits, we developed a selection method for obscured AGN candidates that can be applied to the entire IR sample independently of the availability of X-ray data. The method is based on identifying sources with red and almost featureless near- and mid-IR SED which are evidence for thermal emission from high temperature dust heated by an AGN. Objects with this type of IR SEDs can be identified using the IRAC (3.6, 4.5, 5.8, and 8.0 μm) colors (Lacy et al., 2004; Stern et al., 2004; Hatziminaoglou et al., 2005). Therefore, in order to select AGN among the IR population, we first selected all of the IR sources detected in at least 3 IR bands over the wavelength range 3.6-24μm. This selection reduced the IR sample from 41,262 to 4493 sources. Then we selected sources with a monotonically rising IR (2–24μm) SED, a spectral slope α_{IR} (defined as $F_{\nu} \propto \lambda^{\alpha_{IR}}$) larger than 1.0 and $\chi_{\nu}^{2} < 13.3(\alpha_{IR} - 1) \leq$

20. This selection reduces the sample from 4493 to 248 sources. In order to remove likely unobscured AGN, we then selected all of the sources with optical-IR colors redder than those typical of unobscured quasars, specifically $F(3.6\mu m)/F([g', r', i']) > [15, 13, 10]$. This final criterion is satisfied by 152 sources. The SEDs of these sources were fitted using HYPERZ. Only the sources that could not be fitted with a normal galaxy template at any redshift were kept for a final sample of 100 sources. The final sample of 100 objects was divided in five categories, from I to V. Four categories (I–IV) were defined based on their SED shapes and one category (V) was defined based on the low number (3) of detections in the IR. Category I (12 sources) is characterized by very red IR SEDs with a convex shape. Category II (46 sources) shows power-law like optical-IR SEDs, similar to Mrk 231 or slightly redder (A$_{V}$ <1). Similarly, category III (8 sources) is characterized by power-law like optical-IR SEDs, but not as red as Mrk231; a reddened QSO template (A$_{V}$ =0.3–0.6) provides a better fit. Category IV (21 sources) shows also signatures from an energy source other than the AGN. The SEDs are consistent with templates of composite sources with contributions from both star-formation processes and an AGN component. The SEDs of four sources representatives of categories I to IV are shown in Fig. 2. Category V (13 sources) contains objects with SEDs that are similar to those of the other categories, but they are fainter. A large fraction (44% in total and 91% within 12′ from the center of the radio field) of the selected sources are also detected in the radio. This high radio detection rate supports the hypothesis that these sources are AGN. A small fraction, 32 sources, of the IR-selected obscured AGN candidates are also X-ray detected. Their X-ray spectra show a wide range of hardness ratios, from −0.87 to 0.85, with a median value of −0.27. Since we can not quantify the amount of obscuration in the non X-ray detected sources, we assume that the distribution of absorption in the entire IR-selected sample is similar to that observed in the X-ray detected sub-sample. Only two of these sources (2 out of 32 or 6%) are also present in the X-ray selected sample of Compton-thick AGN (N$_{H}$>10^{24} cm^{-2}), SWIRE_J104409.95+585224.8 (SW104409 hereafter) and SWIRE_J104406.30+583954.1 and their Compton-thick nature is confirmed by their spectroscopic redshifts.

---

[1] http://space.mit.edu/CXC/MARX
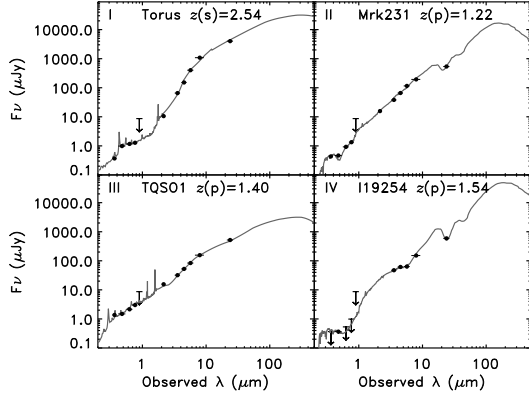[2] HR=(H-S)/(H+S); where H represents the hard (2.5-8 keV) counts and S the soft (0.3-2.5 keV) counts.

Figure 2. SEDs of 4 IR-selected obscured AGN candidates representing 4 different SED categories (I, II, III, IV) as noted on the upper-left corner (see text). Symbols as in Fig. 1.

With this assumption we estimate that 6 out of 100 IR-selected obscured AGN candidates are Compton-thick AGN. One of these two confirmed Compton-thick AGN is analyzed in detail in next section.

4. THE MOST LUMINOUS COMPTON-THICK QSO AT Z≥2

Spectroscopic observations for SW104409 were obtained with the Low Resolution Imaging Spectrometer (LIRS) (Oke et al., 1995) on the Keck I telescope. The optical spectrum, shown in Fig. 3, is characterized by a blue continuum and narrow emission lines (FWHM<1400 $km\,s^{-1}$). A broad, but faint, blue-shifted component is observed in the C IV $\lambda1549$ and N V $\lambda1240$ emission lines. The estimated mean redshift is 2.54±0.02. The SED of SW104409, shown in Fig. 4, is characterized by a rapid rise at longer wavelengths with an observed r'-K_s=4.13 (Vega), fitting the conventional definition of extremely red object (ERO) (Elston et al., 1988). The blue optical continuum and broad line components observed in the optical and the red near-IR SED can be explained by a scenario in which the AGN emission is reddened by dust in the near-IR and completely suppressed at the observed optical wavelengths (ultraviolet in the rest-frame) and the emerging optical emission is due to scattered light. This scenario is represented in Fig. 4 where the SED of SW104409 is compared to the SED of an unobscured QSO template in three cases: 1) normalized at the observed 24μm flux of SW104409 to represent the intrinsic, before absorption, emission of SW104409 (dotted-dashed curve); 2) scaled to match the observed optical data, to represent the scattered component (dashed curve), which corresponds to 0.6% of the intrinsic emission, and 3) reddened by an extinction A_V=4 mag (E(B−V)≃1) (dotted curve). The luminosity as a function of wavelength of SW104409 is shown in Fig. 5. The luminosity distribution of an unob-
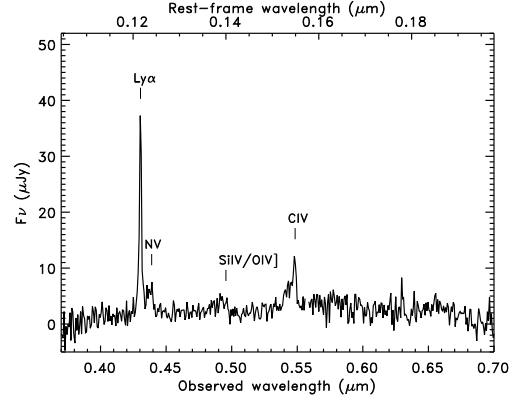

Figure 3. Optical spectrum of SW104409 obtained with the Keck I telescope. Detected emission lines are labeled.

scured QSO template (Elvis et al., 1994) normalized to the mid-IR flux of SW104409 is also shown for comparison. The template is also shown after applying enough extinction A_V to reproduce the red SEDs of SW104409. The integrated optical-IR (0.03–1000μm) luminosity of SW104409 is 3.6×10^{47} $erg\,s^{-1}$ (=9.5×10^{13} $L_\odot$) as derived assuming the model shown in Fig. 4. SW104409 is a hyper-luminous IR galaxy (HYLIRG) (Sanders et al., 1996). The bolometric luminosity, derived by adding the absorption-corrected X-ray luminosity (see Table 1), the radio luminosity (7.9×10^{40} $erg\,s^{-1}$) and the optical-IR luminosity is 3.7×10^{47} $erg\,s^{-1}$. Assuming that the AGN is accreting at the Eddington limit ($L_{bol}=L_{Edd}$), the estimated black-hole mass for SW104409 is $\simeq 2.8 \times 10^9$ $M_\odot$, very similar to the highest measured values in the local Universe, i.e. M87 (Ford et al., 1994) and Cyg A (Tadhunter et al., 2003) ($M_{BH} \simeq 3\times10^9$ $M_\odot$). Note that if the source was accreting below the Eddington limit, the implied black hole mass would be higher.

4.1. Comparison with Compton-thick AGN at $z \geq 2$

Very few high redshift Compton-thick AGN are currently known, including 4 sub-millimeter-selected X-ray sources at z=2–2.5 (Alexander et al., 2005a,b) and 3 X-ray-selected type 2 quasars, CXO-52 (z=3.288) (Stern et al., 2002), CDFS-202 (z=3.700) (Norman et al., 2001), and CDFS-263 (z=3.660) (Mainieri et al., 2005), the latter also being detected in the sub-mm. The sub-mm detected sources show starburst emission in their optical spectra and IR SEDs (Chapman et al., 2005; Borys et al., 2005). The AGN bolometric luminosities, usually only a small fraction of the bolometric luminosity in the sub-set of sub-mm selected AGN, range from 8.4 to 200 $\times10^{44}$ $erg\,s^{-1}$, and the derived black-hole masses range from 0.6 to 11 $\times10^7$ $M_\odot$. The highest luminosity and SMBH mass values belong to the X-ray-selected objects CDFS-202 and CXO-52 which are also optical narrow-line objects, as SW104409. This handful of high-z Compton thick AGN suggests that they represent an
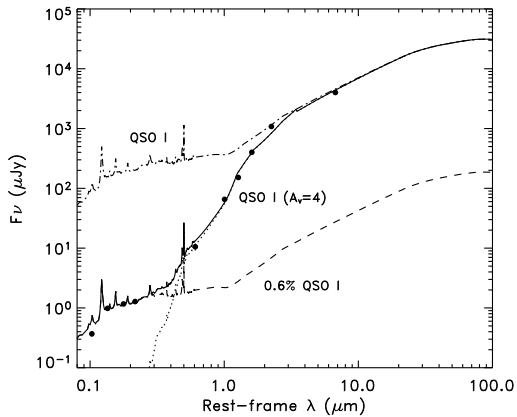
Figure 4. Observed SED of SW104409 (black circles) compared to an unobscured QSO template: 1) normalized to the mid-IR flux of SW104409 (dashed-dotted curve), 2) scaled to match the optical flux of SW104409 (dashed line), and 3) extinguished by $A_V=4$ to fit the IR data points (dotted curve). The solid curve corresponds to the sum of the extinguished (3) and the scattered components (2).
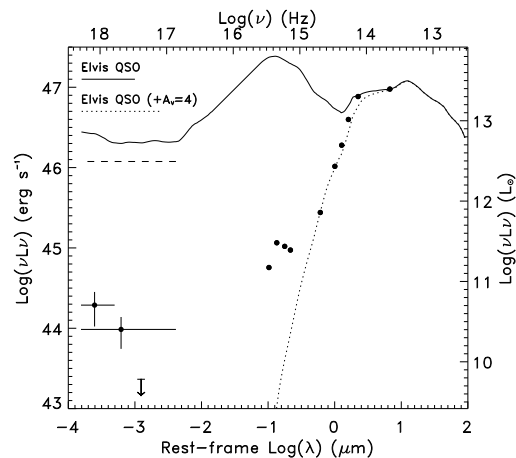

Figure 5. SED in $\nu L\nu$ of SW104409 (black full circles) compared to un unobscured QSO template (Elvis et al., 1994) normalized at 24μm in two cases: 1) with no additional extinction (red solid curve) and 2) with 4.0 mag additional extinction (blue dotted curve). The dashed line corresponds to the absorption-corrected broad band X-ray luminosity.

heterogeneous class with a broad range in luminosity and SMBH masses. The observed differences could be due to a different history or environment, to different evolutionary stages during the AGN obscured phase or to orientation effects.

5. SURFACE DENSITY OF COMPTON-THICK AGN

The two selection methods described in Section 3 were defined to select two samples of obscured AGN based on their X-ray and optical-IR properties, respectively. The X-ray selected sample is biased against Compton-thick AGN whose primary X-ray radiation is completely absorbed in the observed energy range, i.e. sources at low-z or with column densities $\geq 10^{25}$ cm^{-2}, and against sources that are fainter than 10^{-15} ergs cm^{-2} s^{-1} at 0.3-8 keV. The IR-selected sample is biased against AGN that are too faint to be detected in 3 IR bands at our sensitivity limits or whose host galaxy is brighter than the AGN in the optical-IR wavelength range. Since our selection is far from complete, we can only estimate a lower limit to the number of Compton-thick AGN IR detected in the *Chandra*/SWIRE field.

In Section 3.2, we estimate that about 6 sources (6% of 100 sources) among the IR-selected obscured AGN candidates are Compton-thick AGN. Since only two out of five X-ray selected Compton-thick AGN are also selected by the IR-selected criteria, we assume that our IR selection identifies only 40% (2 out of 5) of all Compton-thick AGN in the field. Thus, the estimated total number of Compton-thick AGN in the field is about 15 ($\simeq$6/0.4) sources or 25 per deg^2. The estimated number of sources should be considered a lower limit to the total number of

Compton-thick AGN detected in the IR at our sensitivity limits in the *Chandra*/SWIRE field. Due to the lack of X-ray data for most of the sources, the identification of these 15 Compton-thick AGN is not possible because of lack of constraints on their column densities. The only exceptions are the 5 X-ray selected Compton-thick AGN presented in Section 3.1. The fraction of Compton-thick AGN identified in the X-ray at our depth (F(0.3-8 keV)$\geq$10^{-15} ergs cm^{-2} s^{-1}) is 33% (5 out of 15). This fraction is consistent with the 30% value estimated by Treister et al. (2004) of all Compton-thick AGN detected at the X-ray limit of the *Chandra* deep surveys.

6. SUMMARY

Using the optical/IR/X-ray dataset in the *Chandra*/SWIRE field (0.6 deg^2 in the Lockman Hole), we conducted a search for Compton-thick AGN. Two samples of Compton-thick AGN candidates were independently selected based on their X-ray spectral properties and optical-IR SED. By comparing the properties of the two samples and the fraction of sources selected in both samples, we derive a lower limit to the surface density of Compton-thick AGN detected in the IR to our survey limit of 25 deg^{-2}. We estimate that only 40% of this population shows distinct AGN signatures in their optical-IR SEDs, the rest being dominated by the host-galaxy emission and only 33% of them are identified in the X-ray down to 10^{-15} ergs cm^{-2} s^{-1} broad-band flux limit.

Optical spectroscopy of one candidate, SW104409, confirmed that it is the most luminous Compton-thick QSO at $z > 2$ currently known. The source is characterized by extreme properties, a very red optical-IR spectrum

and $\sim 10^{14} L_\odot$ bolometric luminosity. Such a rare object could be found thanks to the large volumes and the depth of the observations in the SWIRE/*Chandra* field ($\sim 0.6 \deg^2$).

REFERENCES

Alexander, D. M., Bauer, F. E., Chapman et al. 2005a, ApJ, 632, 736

Alexander, D. M., Smail, I., Bauer, F. E. et al. 2005b, *Nature*, 434, 738

Bolzonella M., Miralles J.-M. & Pelló R. 2000, A&A, 363, 476

Borys, C., Smail, I., Chapman, S. C. et al. 2005, ApJ accepted (astro-ph/0507610)

Cattaneo, A., Blaizot, J., Devriendt, J. & Guiderdoni, B. 2005, MNRAS, 359, 1237

Chapman, S. C., Blain, A. W., Smail, I., & Ivison, R. J. 2005, ApJ, 622, 772

Di Matteo, T., Springel, V., & Hernquist, L. 2005, *Nature*, 433, 604

Elston, R., Rieke, G. H. and Rieke, M. J. 1988, ApJ, 331, 77

Elvis, M., Wilkes, B. J., McDowell, J. C. et al. 1994, ApJS, 95, 1

Fabian, A. C. 1999, MNRAS, 308, L39

Fazio, G. G., et al. 2004, ApJS, 154, 10

Ferrarese, L., & Merrit, D. 2000, ApJ, 539, L9

Ford, H.C. et al. 2004, 1994, ApJ, 435, L27

Freeman, P. E., Doe, S., Siemiginowska, A. 2001, *SPIE Proceedings*, 4477, 76

Granato, G., De Zotti, G., Silva, L. et al. 2004, ApJ, 600, 580

Hartwick, F.D.A. 2004, ApJ, 603, 108

Hatziminaoglou, E., Perez-Fournon, I., Polletta M. et al. 2005, AJ, 129, 1198

Hopkins, P. F.,Hernquist, L., Martini, P. et al. 2005, ApJ, 625, 71

La Franca, F. et al. 2005, ApJ, 635

Lacy, M. et al. 2004, ApJS, 154, 166

Leighly, K.M. & Moore, J.R. 2004, ApJ, 611, 107

Longair, M.S. 1992, High Energy Astrophysics, Cambridge, UK: Cambridge University Press

Lonsdale, C. J. et al. 2003, PASP, 115, 897

Lonsdale, C. J., Polletta, M., Surace, J.D. et al. 2004, ApJS, 154, 54

Mainieri, V. et al. 2005, MNRAS, 356, 1571

Maiolino, R., Rieke, G. H., 1995, ApJ, 454, 95

Morrison, R., & McCammon, D. 1983, ApJ, 270, 119

Nandra, K., & Pounds, K. A. 1994, MNRAS, 268, 405

Norman, C. et al. 2002, ApJ, 571, 218

Oke, J. B., Cohen, J. G., Carr, M. et al. 1995, PASP, 107, 375

Piconcelli, E., Cappi, M., et al., 2003, A&A, 412, 689

Rieke, G. et al. 2004, ApJS, 154,

Risaliti, G., Maiolino, R., & Salvati, M. 1999, ApJ, 522, 157

Sanders, D. B., & Mirabel, I. F. 1996, ARA&A, 34, 749

Silk, J. & Rees, M. J. 1998, A&A, 224, L21

Springel, V., Di Matteo, T., & Hernquist, L. 2005, MNRAS, 361, 776

Stern, D. et al. 2002, ApJ, 568, 71

Stern, D. et al. 2005, ApJ, 631, 163

Surace, J. A. et al. 2005, SWIRE Data Delivery Document II, *Spitzer* Science Center, Caltech

Tadhunter, C., Marconi, A., Axon, D. et al. 2003, MNRAS, 342, 861

Treister, E., Urry, C.M., et al., 2004, ApJ, 616, 123

van Dyk, D. A. et al. 2004, HEAD, 8, 1627

Weisskopf, M. C., O'dell, S. L., & van Speybroeck, L. P. 1996, SPIE, 2805, 2

Wolf, C. 2005, MemSAI, 76, 21

Worsley, M. A., Fabian, A. C., Bauer, F. E. et al. 2005, MNRAS, 357, 1281